

Negative Refraction of Infrared Waves and Rays in Sapphire α -Al₂O₃

Noritaka KURODA*[§], Koichi TSUGAWA[‡], and Hiroyuki YOKOI

Department of Materials Science and Engineering, Graduate School of Science and Technology, Kumamoto University, Kumamoto 860-8555, Japan

abstract

The properties of refraction of extraordinary rays at principal surfaces of a uniaxial crystal having a strongly anisotropic dielectric dispersion are studied. Subject to optical nonabsorptivity of the crystal, the criteria for characterizing the refraction behavior are derived from Maxwell's equations. The criteria reveal that in sapphire a variety of specific oblique-incidence reflection spectra arise from negative refraction and counterposition in the infrared region of multimode polar optical phonons. The effects of light dissipation due to damping of the phonons are explored further to interpret the oblique-incidence reflection spectrum measured for the c -surface of a synthetic crystal of sapphire. We pay attention to the directions of wave-normal and Poynting vectors of the infrared light transmitted into the crystal. It turns out that the damping of phonons gives rise to a true negative refraction that the two vectors are simultaneously refracted or deflected negatively in a certain frequency range.

KEYWORDS: negative refraction, counterposition, evanescence, Poynting vector, Brewster's null reflection, Snell's total reflection, LO phonon, sapphire

1. Introduction

Electric field \mathbf{E} , magnetic field \mathbf{H} , and wave vector \mathbf{k} of an electromagnetic plane wave propagating in an isotropic nonabsorbing medium are orthogonal to each other at any instances, since Maxwell's equations for \mathbf{E} , $\mathbf{H} \propto \exp[i(\mathbf{k}\cdot\mathbf{r}-\omega t)]$ give the relationships

$$\mathbf{k} \times \mathbf{E} = \omega\mu\mu_0\mathbf{H}, \quad (1)$$

and

$$\mathbf{H} \times \mathbf{k} = \omega\varepsilon\varepsilon_0\mathbf{E}, \quad (2)$$

where \mathbf{r} , ω and t are the spatial position, angular frequency, and time, respectively; μ and ε are the relative permeability and the dielectric constant of the medium, respectively, and μ_0 and ε_0 are the magnetic permeability and electric permittivity of free space, respectively. In most substances, both μ and ε are positive quantities, and thus \mathbf{E} , \mathbf{H} , and \mathbf{k} form a right-handed triad. Suppose exceptionally that $\mu > 0$ but $\varepsilon < 0$ in a substance, or $\mu < 0$ but $\varepsilon > 0$ in another substance. In the former, if $\mathbf{k} \times \mathbf{E}$ and \mathbf{H} are kept parallel to each other in accord with eq. (1), $\mathbf{H} \times \mathbf{k}$ becomes antiparallel to $\varepsilon\mathbf{E}$ in contradiction to eq. (2), while in the latter, $\mathbf{k} \times \mathbf{E}$ becomes antiparallel to $\mu\mathbf{H}$ in contradiction to eq. (1) if $\mathbf{H} \times \mathbf{k}$ and \mathbf{E} are kept parallel

to each other in accord with eq. (2). Consequently, if either one of ε and μ is negative, no electromagnetic wave can propagate over an arbitrary distance. However, if both of ε and μ are negative, the contradictions between eqs. (1) and (2) are eliminated in turn, and the nonvanishing \mathbf{E} and \mathbf{H} that form a left-handed orthogonal triad with \mathbf{k} are permitted to propagate as the electromagnetic wave.^{1,2,3} The left-handed triad is obtained by reversing the direction of \mathbf{k} of the right-handed triad. In the left-handed system, therefore, the refractive index of light, which is defined by Snell's law for refraction of \mathbf{k} , is negative to cause *negative phase velocity* to plane waves.⁴ In this sense, the left-handed system is called *negative-refractive-index medium*^{2,5}, or the *backward wave medium*^{6,7}.

When a light is obliquely incident into a substance with negative refractive-index, the refraction angle would also be negative. Then \mathbf{k} of the transmitted light would be inclined backward against the interface normal, while pointing in the backward direction as if the light goes out of interior of the substance. Nevertheless, since the energy flow, being given by the Poynting vector $\mathbf{S} = \mathbf{E} \times \mathbf{H}$, is directed antiparallel to \mathbf{k} , the rays of light transmitted into the substance would be deflected backward from the incident

position. To obtain such a negative-refractive-index medium, artificial structures called *metamaterials* have been fabricated by alternately stacking arrays of short conducting wires and small split-ring metallic resonators.⁸⁾ After the proposal of the perfect lens by Pendry⁹⁾ and the experimental verification of the negative refractive index at microwave frequencies by Shelby *et al.*,¹⁰⁾ an enormous amount of studies have been carried out on the optical properties of metamaterials.¹¹⁾

Similar unusual refractions occur in natural crystals with anisotropic structures. In uniaxial crystals ε and μ are tensors of 2nd rank, which have each two principal elements, that is, the elements parallel and normal to the symmetry axes. (Hereafter, these tensors are written as $\hat{\varepsilon}$ and $\hat{\mu}$.) This situation forces \mathbf{S} to be noncollinear with \mathbf{k} . Lindell *et al.* have examined the refraction of *s*-polarized (i.e., transverse electric) and *p*-polarized (i.e., transverse magnetic) light in uniaxial crystals.⁶⁾ Their concern is to see if such a lateral backward deflection of \mathbf{S} as that in metamaterials may take place. They have found that at the *c*-surface at least the *c*-component of either $\hat{\varepsilon}$ or $\hat{\mu}$ should be negative to cause a lateral backward deflection of \mathbf{S} . Subsequently, Belov has examined the refraction of the *p*-polarized light at *a*- and *c*-surfaces of uniaxial dielectric crystals with the *c*-element of $\hat{\varepsilon}$ being negative.⁷⁾ The result demonstrates that at the *a*-surface \mathbf{k} undergoes negative refraction although \mathbf{S} deflects to a forward direction, whereas at the *c*-surface \mathbf{k} undergoes usual positive refraction and \mathbf{S} deflects backward as noticed by Lindell *et al.* To distinguish it from the negative refraction of \mathbf{k} , Lakhtakia and McCall have referred to the latter type of refraction as *counterposition* in view that the vectors \mathbf{k} and \mathbf{S} lie on opposite sides of the surface normal.¹²⁾ Regarding substances exhibiting counterposition as analogues of metamaterials, Narimanov and his coworkers^{13,14)} have proposed exploitation of those substances for the core of a planar wave guide for visible and infrared light. Eritsyan has argued that the counterposition at a plane surface of a crystal functions to focus a diverging light beam.¹⁵⁾ As for the negative refraction in nonmagnetic, anisotropic substances, however, most of the previous studies are in the abstract or of numerical simulation. Furthermore, only a very little efforts have been made so far for spectroscopic studies on unusual refraction phenomena in natural crystals.

Spectroscopically, if ε and μ vary with ω , it

should be in a portion of an originally evanescent frequency region that ε and μ become simultaneously negative to open a spectral transmission window for left-handed waves.³⁾ In the present paper we are concerned with natural compound crystals with uniaxial structures, focusing attention on the refraction of infrared light in the spectral region which is dominated by polar optical phonons. In a uniaxial polar substance the *a*- or *c*-element of $\hat{\varepsilon}$ becomes negative at frequencies in every TO-LO gap, where TO and LO signify the transverse optical and longitudinal optical mode of phonons, respectively. It has been recently found that, if the *p*-polarized light is obliquely incident to the *a* and *c* surfaces of uniaxial binary compounds, a transmission window opens in a certain frequency region in the TO-LO gaps, depending on the angle of incidence.^{16,17)} In the case of sapphire, α -corundum Al_2O_3 , a variety of anomalies appear in the spectrum of oblique-incidence reflection due to multimode optical phonons.¹⁸⁾ These observations strongly suggest that some unusual refractions occur in uniaxial polar substances.

In §2 the propagation of extraordinary rays in the principal configurations of a nonabsorbing uniaxial dielectric crystal are described, where the term nonabsorbing means that $\hat{\varepsilon}$ is a purely real tensor and thus the crystal causes no dissipation of light. On the basis of the result criteria for classifying the refraction properties are derived. It is shown that the angle of incidence, as well as the relative magnitudes and signs of the principal elements of $\hat{\varepsilon}$, is an important ingredient for the refraction behavior of extraordinary rays. In §3 the results of §2 are applied to sapphire. The frequency vs angle-of-incidence diagrams, which show how the counterposition and negative refraction arise as a function of the angle of incidence, are derived in the appropriate frequency regions. To see how the spectral transmission window develops, the spectra of the refractive index, extinction coefficient, and reflectivity are calculated with the angle of incidence taken as the parameter. In §4 the effect of damping of relevant optical phonons are discussed in terms of the properties of the electromagnetic plane wave and the Poynting vector to interpret the practical infrared reflection spectra of sapphire. In §5 an example of the oblique-incidence infrared reflection spectrum newly measured for a synthetic crystal of sapphire at a moderately large angle of incidence is presented. It is shown that the transmission windows are produced by counter-

position and negative refraction in the relevant spectral regions of anisotropic multimode polar optical phonons. On the basis of the present experimental data we evaluate the wave vector and the Poynting vector of the light refracted at the crystal surface to clarify how and in which directions the transmitted waves and rays propagate in the crystal.

2. Electromagnetic Plane Waves in Uniaxial Materials

We are concerned with nonmagnetic, nonabsorbing materials having uniaxial crystal structures. Let the linearly polarized infrared light be incident obliquely from free space to the flat surface of a crystal in principal configurations, as shown in Fig. 1. For a uniaxial crystal, principal configurations may be expressed as sxz or pxz , where s and p signify the s - and p -polarization of light, respectively, whereas x and z are the crystal axes along which the plane of incidence and the surface normal stand, respectively. Since the crystal is optically symmetric under rotation around the c -axis, we may regard any direction within the c -plane as a . Consequently, the principal configurations are represented as sac , pac , saa , paa , sca , and pca .

In general, the linearly polarized plane waves in uniaxial substances are classified into magnetic and electric modes.¹⁹⁾ The light waves in configurations pac , saa , and pca belong to the electric modes. In dielectric, nonmagnetic substances such as sapphire they are extraordinary rays. The isofrequency wave-vector curve of a plane wave propagating in a uniaxial crystal is an ellipse or a hyperbola in configurations pac and pca , depending on the sign combination of the elements of the $\hat{\epsilon}$ tensor, whereas the isofrequency wave-vector curve is a circle in the configuration saa . It is in the configurations pac and pca that the spectral transmission window opens in between the spectral regions of total reflection.¹⁶⁻¹⁸⁾ In the present study, therefore, we are concerned with the refraction of light in the two configurations pac and pca .

The vector \mathbf{n} drawn in Fig. 1 as $\mathbf{n}^{(i)}$, $\mathbf{n}^{(r)}$, and $\mathbf{n}^{(t)}$ represents the wave-normal vector

$$\mathbf{n} = \frac{\mathbf{k}}{k_0}, \quad k_0 = \frac{\omega}{c_0} \quad (3)$$

of incident, reflected, and transmitted waves, respectively, and k_0 and c_0 are the wavenumber and velocity of light in free space, respectively. Here we

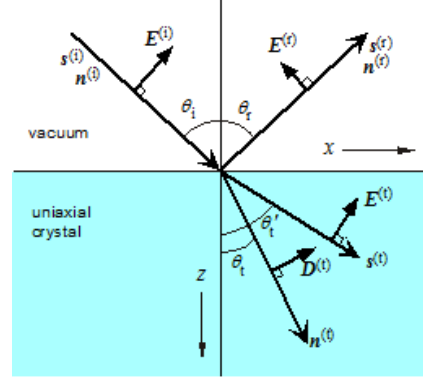


Fig. 1. (Color online) Schematic representation of reflection and refraction of light at a plane surface of a uniaxial crystal.

represent the energy flow density in terms of the ray-index vector \mathbf{s} , which is defined as²⁰⁾

$$\mathbf{s} = \frac{c_0}{c_r} \frac{\mathbf{S}}{S}, \quad (4)$$

where \mathbf{S} is the Poynting vector, and c_r is the ray velocity, that is, the velocity of energy flow of a monochromatic light beam. With respect to the fields $\mathbf{E}^{(t)}$ and $\mathbf{H}^{(t)}$ of the transmitted waves, substitution of $\mathbf{k}^{(t)}$ for \mathbf{k} into eqs. (1) and (2) yields

$$\mathbf{n}^{(t)} \times \mathbf{E}^{(t)} = c_0 \mu_0 \mathbf{H}^{(t)}, \quad (5)$$

and

$$\mathbf{H}^{(t)} \times \mathbf{n}^{(t)} = c_0 \hat{\epsilon} \mathbf{E}^{(t)}, \quad (6)$$

where μ in eq. (1) is taken to be unity since we deal with nonmagnetic crystals, whereas ϵ in eq. (2) is replaced by the tensor $\hat{\epsilon}$.

In pac and pca configurations, by virtue of the continuity of the tangential components of \mathbf{E} and \mathbf{H} at the crystal surface, \mathbf{E} is polarized linearly within the plane of light propagation also in the crystal, whereas \mathbf{H} is directed normal to the plane of light propagation. The light beam is incident at an angle θ_i from free space to the crystal surface; the wave-normal and ray-index vectors, $\mathbf{n}^{(i)}$ and $\mathbf{s}^{(i)}$, are refracted at angles θ_t and θ_t' as drawn in Fig. 1 by $\mathbf{n}^{(t)}$ and $\mathbf{s}^{(t)}$, respectively. Vectors $\mathbf{n}^{(t)}$ and $\mathbf{s}^{(t)}$ are not collinear, and $\mathbf{s}^{(t)}$ is related to $\mathbf{n}^{(t)}$ as²⁰⁾

$$\mathbf{s}^{(t)} = \mathbf{n}^{(t)} \cos(\theta_t' - \theta_t). \quad (7)$$

Since the displacement $\mathbf{D}^{(t)}$ is given by $\mathbf{D}^{(t)} = \hat{\epsilon} \mathbf{E}^{(t)}$, θ_t' is related to θ_t as

$$\tan \theta_t' = \frac{\epsilon_x}{\epsilon_z} \tan \theta_t, \quad (8)$$

with ε_x and ε_z being xx and zz elements of $\hat{\varepsilon}$, respectively. We find from eq. (8) that the unusual refraction phenomena mentioned in §1 arise generally when ε_x and ε_z have opposite signs. From the law of conservation of momentum, the transverse component of \mathbf{k} , that is, k_x , is conserved upon refraction. The same is true of \mathbf{n} , yielding Snell's law

$$\sin\theta_i = n_x^{(i)} = n^{(i)}\sin\theta_t . \quad (9)$$

The dispersion equation for electric modes in *pac* and *pca* configurations¹⁹⁾ leads to Fresnel's equation, which relates $n^{(i)}$ with θ_t as

$$\frac{\sin^2\theta_t}{\varepsilon_z} + \frac{\cos^2\theta_t}{\varepsilon_x} = \frac{1}{n^{(i)2}} . \quad (10)$$

In the present study, in order to permit $n^{(i)}$ to explicitly bear the sign, we restrict the variation of θ_t to the range $-90^\circ \leq \theta_t \leq 90^\circ$. As regards the ray refractive angle θ_t' it is postulated that $-90^\circ \leq \theta_t' \leq 90^\circ$ since the refracted ray carries energy into the crystal. In the case of $\theta_t = \theta_t' = \pm 90^\circ$ the refracted light wave is purely evanescent.

With the aid of eqs. (8), (9), and (10) we find that eq. (5) yields

$$n_z^{(i)}E_x^{(i)} = c_0\mu_0\left(1 - \frac{\sin^2\theta_t}{\varepsilon_x}\right)H_y^{(i)} . \quad (11)$$

Turning attention to eq. (6), we obtain

$$n_z^{(i)}H_y^{(i)} = c_0\varepsilon_x\varepsilon_0E_x^{(i)} . \quad (12)$$

The fields $E_x^{(i)}$ and $H_y^{(i)}$ are oscillating synchronously, but the z component $E_x^{(i)}H_y^{(i)*}$ of the stationary part of the Poynting vector $\mathbf{S} = \mathbf{E}^{(i)} \times \mathbf{H}^{(i)}$ is always positive. Consequently, it emerges from eqs. (11) and (12) that the factors $1 - \sin^2\theta_t/\varepsilon_x$ and ε_x are crucial for determining $n_z^{(i)}$ just like μ and ε determining $n^{(i)}$ to be $\sqrt{\mu}\sqrt{\varepsilon}$ in the case of an isotropic metamaterial. Taking account of signs of the two factors, we find that Mosteller and Wooten's early expression of the wave-normal vector²¹⁾ is valid even for unusual refractions. From Fresnel's equation (10) and Snell's law (9), in accordance with eq. (39) of ref. 21, we can write $\mathbf{n}^{(i)}$ as

$$\mathbf{n}^{(i)} = n_x^{(i)}\mathbf{x} + n_z^{(i)}\mathbf{z} , \quad (13)$$

with

$$n_z^{(i)} = \sqrt{\varepsilon_x} \sqrt{1 - \frac{\sin^2\theta_t}{\varepsilon_z}} , \quad (14)$$

where \mathbf{x} and \mathbf{z} are unit vectors along x and z axes, respectively. This finding gives the following criteria for characterizing the refraction behavior:

(a) When $1 - \sin^2\theta_t/\varepsilon_z$ and ε_x are simultaneously positive, $n^{(i)}$ is positive, being given by

$$n^{(i)} = \sqrt{\sin^2\theta_t + \varepsilon_x\left(1 - \frac{\sin^2\theta_t}{\varepsilon_z}\right)} . \quad (15)$$

If $\varepsilon_z > \sin^2\theta_t$, both θ_t and θ_t' are positive as they are in the usual refraction. When $\varepsilon_z < 0$, we still have $\theta_t > 0$, but eq. (8) claims that $\theta_t' < 0$. The latter is the counterposition of the wave-normal and ray-index vectors.

(b) When $1 - \sin^2\theta_t/\varepsilon_z$ and ε_x are simultaneously negative, that is, $0 < \varepsilon_z < \sin^2\theta_t$ and $\varepsilon_x < 0$, $n_z^{(i)}$ is negative to give

$$n^{(i)} = -\sqrt{\sin^2\theta_t + \varepsilon_x\left(1 - \frac{\sin^2\theta_t}{\varepsilon_z}\right)} . \quad (16)$$

Although $\theta_t < 0$, we see that $\theta_t' > 0$ from eq. (8), so that the rays of light penetrate into the crystal toward a positive direction of x .

(c) When either $1 - \sin^2\theta_t/\varepsilon_z$ or ε_x is negative, $n_z^{(i)}$ is imaginary, so that the refracted light wave is evanescent. Then, the refracted wave propagates along the surface without penetrating into the crystal. If $\varepsilon_x > 0$ and $0 < \varepsilon_z < \sin^2\theta_t$, or $\varepsilon_x < 0$ and $\varepsilon_z > \sin^2\theta_t$, Snell's total reflection (STR) occurs. When both ε_x and ε_z are negative, the crystal behaves as a metal-like reflector.

It turns out from above considerations that the unusual refractions, that is, negative refraction and counterposition, take place when $1 - \sin^2\theta_t/\varepsilon_z$ and ε_x are simultaneously positive or negative providing that ε_x and ε_z have opposite signs, namely $\hat{\varepsilon}$ is *indefinite*²²⁾. What is different from the case of isotropic metamaterials is that the properties of refraction depend essentially on the angle of incidence

of light. In unusual refractions, either wavevector or ray alone is refracted or deflected negatively. Another point is the frequency dependence of ε_x and ε_z . Supposed that ε_x and ε_z are increasing functions of frequency with zeros at each individual frequencies, either negative refraction or counterposition is predicted to appear near the zeros in between evanescent regions.

In connection with these unusual refractions Brewster's law plays an important role in the infrared spectrometry, producing null reflections at $(\theta, \omega) = (\theta_B, \omega_B)$ satisfying^{18, 23)}

$$\frac{\varepsilon_x(\omega_B) - 1}{\varepsilon_z(\omega_B) - 1} \varepsilon_z(\omega_B) = \tan^2 \theta_B. \quad (17)$$

Not only when both ε_x and ε_z are positive, but also when they are in opposite signs, a solution (θ_B, ω_B) may exist to eq. (17). This Brewster's null reflection (BNR) has been the subject of recent studies of small-angle oblique-incidence reflectometry in ZnO¹⁷⁾ and sapphire¹⁸⁾.

3. Refraction of Lattice-Vibrational Infrared Light in Sapphire

The primitive unit cell of the α -corundum structure of sapphire belongs to the D_{3d} point group and yields the following normal modes of lattice vibration:²⁴⁾

$$\Gamma = 2A_{1g} + 2A_{1u} + 3A_{2g} + 3A_{2u} + 5E_g + 5E_u. \quad (18)$$

Among these normal modes, two representations of A_{2u} and four representations of E_u are infrared-active optical modes polarized parallel and perpendicular to the c -axis, respectively. Each infrared-active optical mode produces a pair of TO and LO phonon branches. In Gervais and Piriou's FPSQ oscillator model²⁵⁾, the principal dielectric functions are given by

$$\varepsilon_{\parallel(\perp)}(\omega) = \varepsilon_{\infty\parallel(\perp)} \prod_j \frac{\omega_{LO_{\parallel(\perp)}^j}^2 - \omega^2 - i\gamma_{LO_{\parallel(\perp)}^j} \omega}{\omega_{TO_{\parallel(\perp)}^j}^2 - \omega^2 - i\gamma_{TO_{\parallel(\perp)}^j} \omega}, \quad (19)$$

where $\varepsilon_{\parallel}(\omega)$ and $\varepsilon_{\perp}(\omega)$ are the principal elements of $\hat{\varepsilon}$ for the directions of \mathbf{E} and \mathbf{D} parallel to c and a axes, respectively, ε_{∞} is the optical dielectric constant, $\omega_{LO(TO)}$ is the frequency of the LO(TO) phonon, and $\gamma_{LO(TO)}$ is the damping energy of the LO(TO) phonon. Two LO_{\parallel}^j (TO_{\parallel}^j)'s with $j = 1$ and 2 signify two LO(TO) phonons of the A_{2u} modes, whereas four

Table I. Frequencies (cm^{-1}) of polar optical modes in sapphire. Numbers in parentheses are the damping energies (cm^{-1}).

Representation	TO	LO
A_{2u}^1	398.0 (5.7)	511.0 (1.5)
A_{2u}^2	583.0 (2.5)	879.4 (25)
E_u^1	384.6 (4.8)	387.7 (4.8)
E_u^2	439.3 (4.8)	481.2 (1.8)
E_u^3	569.5 (4.5)	629.2 (6.5)
E_u^4	633.5 (5.2)	908.5 (18)

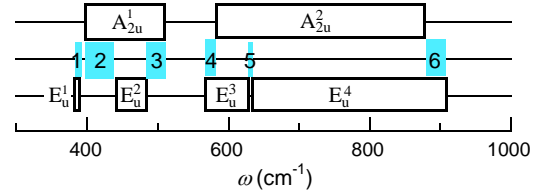


Fig. 2. (Color online) TO-LO bands of two A_{2u} and four E_u modes of polar optical phonons in sapphire. The areas numbered 1 through 6 are the frequency regions in which ε_{\parallel} and ε_{\perp} have opposite signs.

Table II. Type of refraction in configurations pac and pca in the frequency regions 1 through 6.

Frequency region	Type of refraction	
	pac	pca
1	Evanescence	Counterposition
2	Counterposition	Evanescence
3	Counterposition	Negative Refraction* ¹
4	Evanescence	Counterposition
5	Counterposition	Negative Refraction* ²
6	Negative Refraction* ³	Counterposition

*¹The upper bound of the negative refraction region is S_{\perp}^2 when S_{\perp}^2 lies below LO_{\perp}^1 .

*²The upper bound of the negative refraction region is S_{\perp}^3 .

*³The upper bound of the negative refraction region depends on θ . See text of §3.2.

LO_{\perp}^j (TO_{\perp}^j)'s with $j = 1 - 4$ signify four LO(TO) phonons of the E_u modes. Table I lists the frequencies and damping energies of those phonons obtained from recent infrared experiment¹⁸⁾ and the present work described in §5. The values of $\varepsilon_{\infty\parallel}$ and $\varepsilon_{\infty\perp}$ are known to be 3.038 and 3.064, respectively.²⁶⁾ In this Section, to keep consistency with the argument in §2, the

damping energies, γ 's, are assumed to be vanishingly small unless otherwise noted. Within the framework of this assumption, ε_{\parallel} and ε_{\perp} are purely real and positive outside the TO-LO gap of every A_{2u} and E_u mode, respectively, while ε_{\parallel} and ε_{\perp} are purely real and negative inside the gap of every A_{2u} and E_u mode, respectively. The point to be noted is that ε_{\parallel} and ε_{\perp} diverge to $\pm\infty$ at the frequencies of TO_{\parallel}^j and TO_{\perp}^j , and then go up through zeros at the frequencies of LO_{\parallel}^j and LO_{\perp}^j , respectively, as ω increases.

There are six regions of frequency where ε_{\parallel} and ε_{\perp}

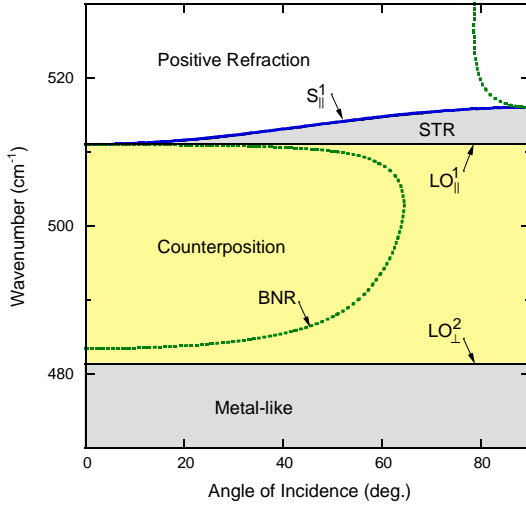


Fig. 3. (Color online) Diagram of refraction properties of sapphire in the θ_1 - ω coordinates in the *pac* configuration around the frequency region 3.

have opposite signs as shown in Fig. 2. In the *pac* configuration we have $\varepsilon_x = \varepsilon_{\perp}$ and $\varepsilon_z = \varepsilon_{\parallel}$, while in the *pca* configuration we have $\varepsilon_x = \varepsilon_{\parallel}$ and $\varepsilon_z = \varepsilon_{\perp}$. Table II summarizes the results of application of the criteria (a), (b), and (c) given in §2 to the *pac* and *pca* configurations in the six regions of frequency. In the followings, as the representative example of counterposition and negative refraction, we look closely at the refraction properties around the regions 3 and 6, respectively, in the *pac* configuration.

3.1 Counterposition in region 3

The region 3 ranges from 481.2 cm^{-1} of LO_{\perp}^2 to 511.0 cm^{-1} of LO_{\parallel}^1 . In this region we have $\varepsilon_{\perp} > 0$ but $\varepsilon_{\parallel} < 0$, so that there should occur counterposition in the configuration *pac*. Figure 3 illustrates the diagram of refraction in the θ_1 - ω coordinates covering the region 3. In Fig. 4 are shown the spectra of the real and imaginary $n_z^{(i)}$, signified by $n_z^{(i)'}$ and $n_z^{(i)''}$, respectively, around the region 3 at $\theta_1 = 20^\circ$, for

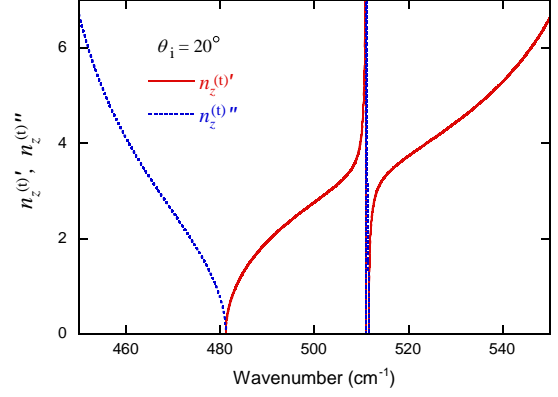


Fig. 4. (Color online) $n_z^{(i)'}$ and $n_z^{(i)''}$ at $\theta_1 = 20^\circ$ in the configuration *pac* in the neighborhood of the frequency region 3 of sapphire.

example. Since the damping energies are assumed to be negligibly small here, $n_z^{(i)}$ is either purely real or purely imaginary at any frequencies. Note that the region 3 is sandwiched between evanescent regions. The width of the evanescent region due to STR on the higher frequency side is vanishingly small at $\theta_1 = 0$, but enlarges as θ_1 increases. This is because the region of the frequency satisfying $1 - \sin^2 \theta_i / \varepsilon_{\parallel} < 0$ with $\varepsilon_{\parallel} > 0$ widens as θ_1 increases. The boundary is determined by the polariton state S_{\parallel}^1 of which the frequency ω_S is given by

$$\varepsilon_{\parallel}(\omega_S) = \sin^2 \theta_1. \quad (20)$$

We can calculate the isofrequency curve of wave-normal vector from eq. (10). Figure 5 shows the curves in free space and the sapphire crystal at a frequency $\omega = 483.8 \text{ cm}^{-1}$ in the region 3. At this value of ω eq. (19) gives $\varepsilon_{\parallel} = -5.534$ and $\varepsilon_{\perp} = 1.157$, with which eq. (17) yields Brewster's angle θ_B to be 20° . The curve in the sapphire crystal is a hyperbola with its main axis lying normal to the surface of the crystal. The vectors $\mathbf{n}^{(i)}$, $\mathbf{s}^{(i)}$, $\mathbf{n}^{(t)}$, and $\mathbf{s}^{(t)}$ at $\omega = 483.8 \text{ cm}^{-1}$ and $\theta_1 = 20^\circ$ are drawn along with the isofrequency curves. Note that $\mathbf{s}^{(t)}$ is deflected to a backward direction although $\mathbf{n}^{(t)}$ is refracted to a forward direction in a usual way.

To grasp the role of counterposition we shall now survey the reflection spectrum. The reflectivity for the configuration *pac* is given by^{18, 21)}

$$R = \frac{\left| \sqrt{\varepsilon_{\parallel}(\omega)\varepsilon_{\perp}(\omega)} \cos \theta_i - \sqrt{\varepsilon_{\parallel}(\omega) - \sin^2 \theta_i} \right|^2}{\left| \sqrt{\varepsilon_{\parallel}(\omega)\varepsilon_{\perp}(\omega)} \cos \theta_i + \sqrt{\varepsilon_{\parallel}(\omega) - \sin^2 \theta_i} \right|^2}. \quad (21)$$

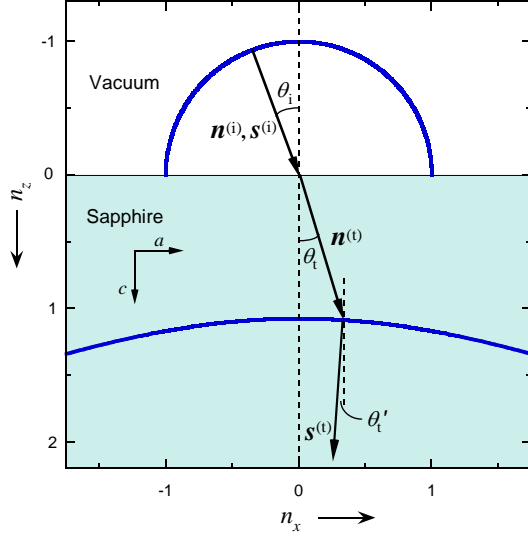


Fig. 5. (Color online) Isofrequency curves of wave-normal vector at 483.8 cm^{-1} in vacuum and sapphire in the *pac* configuration. To make an intuitive correspondence to the refraction scheme shown in Fig. 1, the curves are drawn only in the negative and positive sides of the ordinate for free space and the sapphire crystal, respectively. The vectors $\mathbf{n}^{(i)}$ and $\mathbf{s}^{(i)}$ show that light is incident at Brewster's angle $\theta_B = 20^\circ$, while $\mathbf{n}^{(t)}$ and $\mathbf{s}^{(t)}$ show wave-normal and ray-index vectors, respectively, of the refracted light.

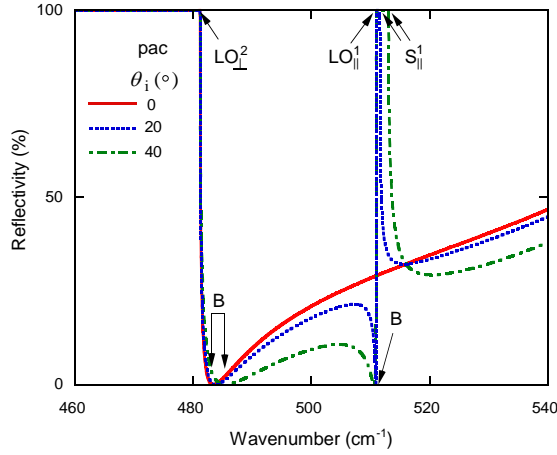


Fig. 6. (Color online) Variation with θ_i of the reflectivity spectrum around the region 3 in the configuration *pac*. Null reflections due to BNR are indicated by the arrows B.

Figure 6 shows the reflection spectra calculated for $\theta_i = 0^\circ, 20^\circ$, and 40° . For the normal incidence of $\theta_i = 0^\circ$, the total reflection starting from TO_\perp^2 lasts up to LO_\perp^2 : With increasing ω beyond LO_\perp^2 the reflectivity drops down rapidly to become null at the frequency 483.4 cm^{-1} which satisfies $\epsilon_\perp = 1$, and then rises again toward the resonance with TO_\perp^3 located at

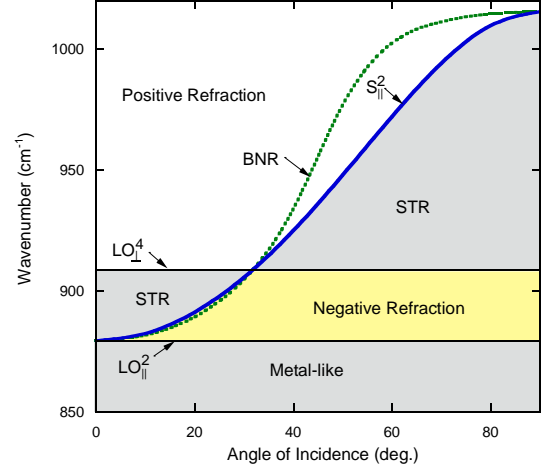


Fig. 7. (Color online) $\theta_i - \omega$ diagram of refraction in sapphire around the region 6 in the configuration *pac*.

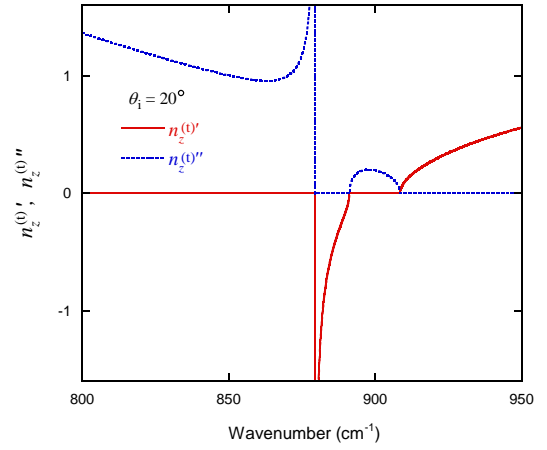


Fig. 8. (Color online) $n_z^{(t)'}$ and $n_z^{(t)''}$ at $\theta_i = 20^\circ$ in sapphire around the frequency region 3 in the configuration *pac*.

569.5 cm^{-1} . For $\theta_i > 0^\circ$, this null reflection is transformed into BNR, and ω_B increases gradually from 483.4 cm^{-1} with increasing θ_i . At the same time, another BNR appears at a frequency just below LO_\parallel^1 . In addition, the aforementioned evanesence band develops from the edge of LO_\parallel^1 up to the frequency of S_\parallel^1 . The two null reflections due to BNR come up to one another as θ_i increases. As a result, the reflectivity inside the region 3 diminishes, and thus the power of the incident light is transmitted more and more into the crystal as θ_i increases.

3.2 Negative refraction in region 6

Figure 7 shows the $\theta_i - \omega$ diagram of refraction around the region 6 in the *pac* configuration. In the region 6 we have $\epsilon_\parallel > 0$ but $\epsilon_\perp < 0$, so that there should

occur negative refraction. At $\theta_i = 0^\circ$, however, the crystal behaves as a metal-like total reflector for frequencies up to 879.4 cm^{-1} of LO_\parallel^2 , and then undergoes STR up to 908.5 cm^{-1} of LO_\perp^4 since, in accord with the criterion (c) given in §2, $1 - \sin^2 \theta_i / \varepsilon_\parallel$ and ε_\perp have opposite signs such that $1 - \sin^2 \theta_i / \varepsilon_\parallel = 1$ and $\varepsilon_\perp < 0$. When $\theta_i > 0^\circ$ a transmission window due to negative refraction opens in the frequency range satisfying $0 < \varepsilon_\parallel < \sin^2 \theta_i$. The width of the transmission window increases with increasing θ_i : The upper bound of this transmission window scales with θ_i as the frequency of the polariton state S_\parallel^2 until reaching LO_\perp^4 at $\theta_i = 31.7^\circ$. Figure 8 shows the spectra of $n_z^{(i)}$ and $n_z^{(t)}$ at $\theta_i = 20^\circ$. The alternate change in the spectral region from metal-like evanescence through normal positive refraction with increasing frequency is illustrated clearly. If θ_i exceeds 31.7° the upper bound of negative refraction is pinned to LO_\perp^4 . At frequencies above LO_\perp^4 up to S_\parallel^2 , the signs of the discrimination parameters are reversed such that $1 - \sin^2 \theta_i / \varepsilon_\parallel < 0$ and $\varepsilon_\perp > 0$, and therefore STR causes evanescence.

Figure 9 shows the isofrequency curves of wave-normal vector for $\omega = 889.3 \text{ cm}^{-1}$. The curves for sapphire are obtained from the values of $\varepsilon_\parallel = 0.098$ and $\varepsilon_\perp = -0.215$. In this case the main axis of the hyperbola is parallel to the crystal surface. We note, therefore, that the refraction is possible only for $\theta_i \geq 18.5^\circ$, consistent with the argument given in the preceding paragraph. Taking into account that at this frequency Brewster's angle θ_B is 20° , vectors $\mathbf{n}^{(i)}$, $\mathbf{s}^{(i)}$, $\mathbf{n}^{(t)}$, and $\mathbf{s}^{(t)}$ for $\theta_i = 20^\circ$ are drawn along with the isofrequency curves. It is obvious that \mathbf{n} undergoes a negative refraction, and \mathbf{s} is deflected to a forward direction. In Fig. 10 are shown the vectors $\mathbf{D}^{(t)}$ and $\varepsilon_0 \mathbf{E}^{(t)}$ of the plane wave at the surface of the crystal under this Brewster condition. Their magnitudes are normalized with $\varepsilon_0 \mathbf{E}^{(i)}$ of the incident light at the crystal surface. Because of negative refractive index of $n^{(t)} = -0.397$, $\mathbf{D}^{(t)}$ points in a direction on the side of negative x , subtending an angle of $|\theta_t| \approx 60^\circ$ from the crystal surface. Then the relationship $\varepsilon_0 \mathbf{E}^{(t)} = \hat{\varepsilon}^{-1} \mathbf{D}^{(t)}$ with $\varepsilon_\parallel^{-1} \approx 10$ and $\varepsilon_\perp^{-1} \approx -5$ forces $\varepsilon_0 \mathbf{E}^{(t)}$ to upturn steeply from the crystal surface, while inclining toward the positive x direction. The produced polarization vector $\mathbf{P}^{(t)} = \mathbf{D}^{(t)} - \varepsilon_0 \mathbf{E}^{(t)}$ is inclined at 20° , being equal to θ_B , against the surface normal, in accordance with Brewster's law.²⁷⁻²⁹⁾

Figure 11 shows the reflection spectra calculated from eq. (23) for θ_i of 0° , 20° and 40° . At $\theta_i = 0^\circ$, the

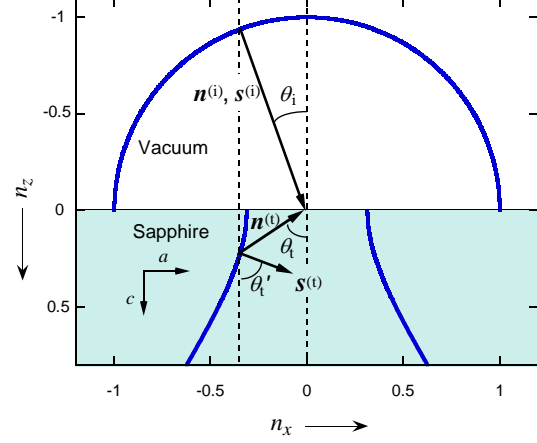


Fig. 9. (Color online) Isofrequency curves of wave-normal vector at 889.2 cm^{-1} in vacuum and sapphire in the *pac* configuration. To make an intuitive correspondence to the refraction scheme shown in Fig. 1, the curves are drawn only in the negative and positive sides of the ordinate for free space and the sapphire crystal, respectively. The vectors $\mathbf{n}^{(i)}$ and $\mathbf{s}^{(i)}$ show that light is incident at Brewster's angle $\theta_B = 20^\circ$, while $\mathbf{n}^{(t)}$ and $\mathbf{s}^{(t)}$ are the wave-normal and ray-index vectors, respectively, of the refracted light.

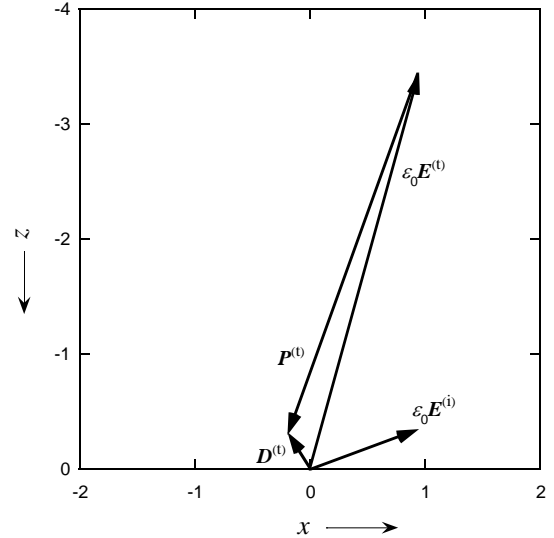


Fig. 10. Displacement and polarization vectors at the surface of the sapphire crystal under Brewster's condition illustrated in Fig. 9. The magnitude of the displacement vectors $\mathbf{D}^{(t)}$, $\varepsilon_0 \mathbf{E}^{(t)}$, and $\mathbf{P}^{(t)}$ in sapphire are normalized with the magnitude of $\varepsilon_0 \mathbf{E}^{(i)}$ in vacuum.

total reflection lasts up to the frequency 908.5 cm^{-1} of LO_\perp^4 . The spectra for $\theta_i = 20^\circ$ and 40° demonstrate that a transmission window opens above LO_\parallel^2 , and widens with increasing θ_i ; for $\theta_i > 31.7^\circ$ the window covers the whole range of region 6 to connect to the STR region which is bounded by S_\parallel^2 . In accord with

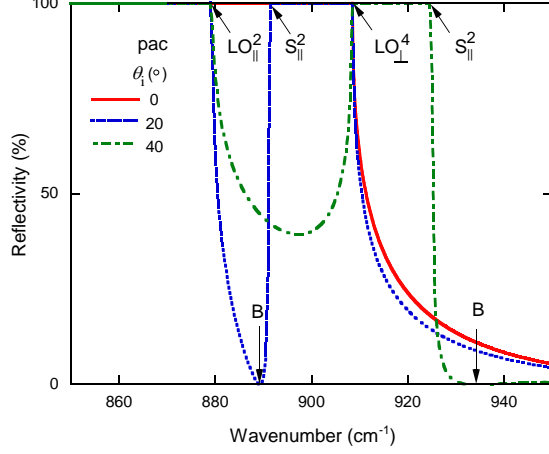


Fig. 11. (Color online) Variation of the reflectivity spectrum around the frequency region 6 with θ_1 in the configuration *pac*. Null reflections due to BNR are indicated by the arrows B.

the refraction diagram of Fig. 7, Brewster's null reflection (BNR) occurs inside the transmission window for $\theta_1 < 31.7^\circ$, while moving outside the STR region for $\theta_1 > 31.7^\circ$.

3.3 Positive refraction outside region 6

For comparison with the case of negative refraction described above, Fig. 12 shows the isofrequency curves of wave-normal vector for positive refraction at a frequency outside the region 6. The frequency is chosen to be 934.1 cm^{-1} in order to set Brewster's angle to be 40° . Since both of $\varepsilon_{\parallel} = 0.484$ and $\varepsilon_{\perp} = 0.251$ at this frequency are positive, the curve of sapphire is elliptic. Vectors $\mathbf{n}^{(i)}$, $\mathbf{s}^{(i)}$, $\mathbf{n}^{(t)}$, and $\mathbf{s}^{(t)}$ for $\theta_1 = 40^\circ$ are drawn along with the isofrequency curves. Note that the critical angle of incidence for STR is 44.8° , and that as long as $0 < \theta_1 < 44.8^\circ$, vectors $\mathbf{n}^{(t)}$ and $\mathbf{s}^{(t)}$ are non-collinear irrespective of θ_1 .

4. Effect of Damping

Optical phonons of sapphire inherently have significant levels of damping which cause ε_{\parallel} and ε_{\perp} to be complex.^{18,25} The imaginary parts of ε_{\parallel} and ε_{\perp} function to relax the conditions for discriminating the type of refraction, and enlarge in turn the variety of unusual refractions.³⁰ As stressed by Markel and Schotland,³¹ the power dissipation of light caused by the imaginary part of dielectric constants is an important ingredient for practical applications of negative refraction.

When ε_x and ε_z are complex, $n_z^{(t)}$ is also

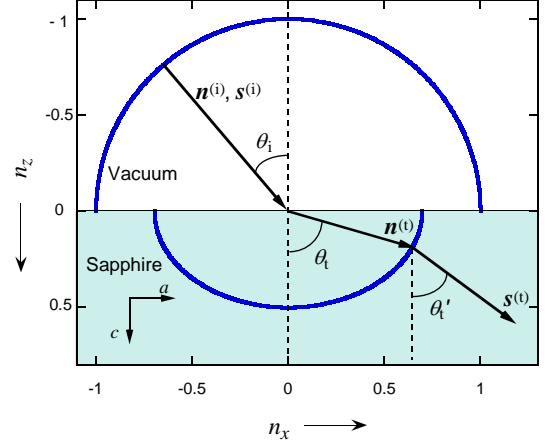


Fig. 12. (Color online) Isofrequency curves of wave-normal vector at 934.1 cm^{-1} in vacuum and sapphire in the *pac* configuration. To make an intuitive correspondence to the refraction scheme shown in Fig. 1, the curves are drawn only in the negative and positive sides of the ordinate for free space and the sapphire crystal, respectively. The vectors $\mathbf{n}^{(i)}$ and $\mathbf{s}^{(i)}$ show that light is incident at Brewster's angle $\theta_B = 40^\circ$, while $\mathbf{n}^{(t)}$ and $\mathbf{s}^{(t)}$ are the wave-normal and ray-index vectors, respectively, of the refracted light.

complex, so that we can write

$$n_z^{(t)} = n_z^{(t)'} + i n_z^{(t)''}. \quad (22)$$

The nonvanishing imaginary part $n_z^{(t)''}$ causes refracted waves to be inhomogeneous, and thus to be evanescent in a general sense. In this case, the real part $n_z^{(t)'}$ permits the refracted waves to penetrate into the crystal. Following the procedure of Mosteller and Wooten²¹ for treating Maxwell's equations in absorbing uniaxial crystals, the electromagnetic fields of the refracted light in the configurations *pac* and *pca* are given by

$$\mathbf{E}^{(t)} = \frac{H_{y0}^{(i)} \phi}{c_0 \varepsilon_0} \left[\frac{n_z^{(t)}}{\varepsilon_x} \mathbf{x} + \frac{\sin \theta_1}{\varepsilon_z} \mathbf{z} \right] \exp \{ -n_z^{(t)''} k_0 z + i [k_0 (\sin \theta_1 x + n_z^{(t)'} z) - \omega t] \},$$

$$\mathbf{H}^{(t)} = H_{y0}^{(i)} \phi \exp \{ -n_z^{(t)''} k_0 z + i [k_0 (\sin \theta_1 x + n_z^{(t)'} z) - \omega t] \}, \quad (23)$$

with

$$\phi = \frac{2 \varepsilon_x \cos \theta_1}{n_z^{(t)} + \varepsilon_x \cos \theta_1}, \quad (24)$$

where $H_{y0}^{(i)}$ is the value of $H_y^{(i)}$ at the origin on the crystal surface, and \mathbf{y} is the unit vector along the y axis. Hence the time-averaged Poynting vector $\bar{\mathbf{S}}^{(i)}$ is given by

$$\begin{aligned}\bar{\mathbf{S}}^{(i)} &= \frac{1}{2} \text{Re}[\mathbf{E}^{(i)} \times \mathbf{H}^{(i)*}] \\ &= \frac{|H_{y0}^{(i)}|^2 |\phi|^2}{2c_0 \varepsilon_0} \text{Re}\left[\frac{\sin \theta_i}{\varepsilon_z} \mathbf{x} \right. \\ &\quad \left. + \frac{n_z^{(i)}}{\varepsilon_x} \mathbf{z}\right] \exp[-2n_z^{(i)''} k_0 z].\end{aligned}\quad (25)$$

Here, we obtain the real angle of refraction from

$$\tan \theta_t = \frac{\sin \theta_i}{n_z^{(i)'}}. \quad (26)$$

The real refractive index can be expressed as

$$n^{(i)} = n_z^{(i)'} \sqrt{1 + \frac{\sin^2 \theta_i}{n_z^{(i)'^2}}}, \quad (27)$$

showing that the sign of $n_z^{(i)'}$ determines the sign of $n^{(i)}$. With respect to the deflection of the rays of light we see from eq. (25) that

$$\tan \theta_t' = \frac{\text{Re}\left[\frac{\sin \theta_i}{\varepsilon_z}\right]}{\text{Re}\left[\frac{n_z^{(i)'}}{\varepsilon_x}\right]}, \quad (28)$$

corresponding to eq. (8) for nonabsorbing crystals. Bringing to mind that the denominator of the right hand side of eq. (28) comes from the z -component of $\bar{\mathbf{S}}^{(i)}$, and thus is always positive, the rays are found to exhibit negative deflection whenever $\text{Re}(\varepsilon_z) < 0$, irrespective of the sign of ε_x . This is an example of the relaxation of refraction criteria due to damping.

We see from eqs. (23) and (25) that the wave fronts of constant amplitude of electromagnetic fields are the planes $n_z^{(i)''} k_0 z = \text{constant}$ and the fronts of the constant intensity of light are the planes $2n_z^{(i)''} k_0 z = \text{constant}$. Let us now look at the spectra of $n_z^{(i)'}$ and the absorption coefficient

$$\alpha = 2n_z^{(i)''} k_0 \quad (29)$$

for $\theta_i = 25^\circ$ in the *pac* configuration by introducing practical damping energies of phonons listed in Table I into eq. (19) for ε_\perp and ε_\parallel . The value 25° of θ_i is chosen so as to be consistent with the experiment

described in §5. Figures 13(a) and 13(b) show the spectra of $n_z^{(i)'}$ and α at frequencies around the regions 3 and 6, respectively. As expected, damping energies cause the boundaries between the spectral regions of propagating and evanescent waves to become significantly obscure. The result around region 3 shown in Fig. 13(a) agrees substantially with the behavior shown in Fig. 4, since the damping energies of the phonons LO_\perp^2 and LO_\parallel^1 are comparatively small. As for the result around region 6 shown in Fig. 13(b), the structures of metal-like evanescence and STR, which are expected to appear in the α spectrum just below LO_\parallel^2 and between S_\parallel^2 and LO_\perp^4 , respectively (see Fig. 8), if the damping of LO_\parallel^2 and LO_\perp^4 is small, are strongly obscured. As a consequence, the influence of absorption extends over the region of original negative refraction. The spectral negative peak of $n_z^{(i)'}$ is also suppressed and broadened, so that the frequency region of negative refraction expands to the lower frequency side of LO_\parallel^2 .

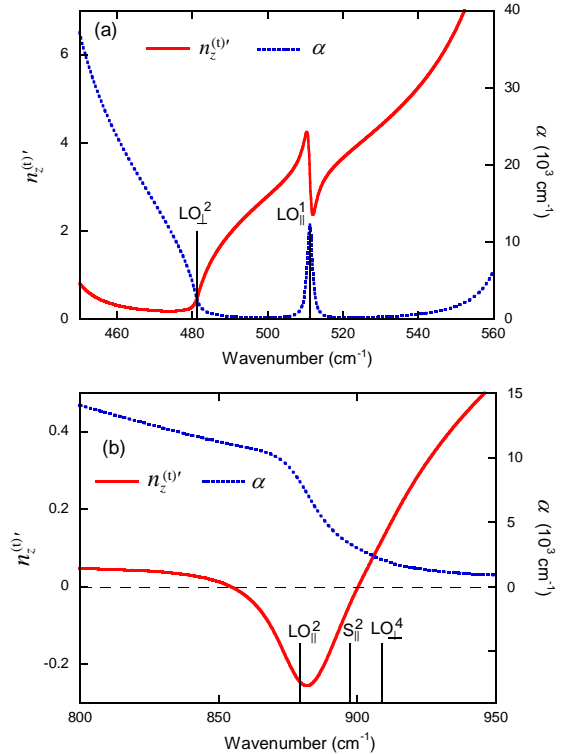


Fig. 13. (Color online) $n_z^{(i)'}$ and α in sapphire for $\theta_i = 25^\circ$ in the configuration *pac* around (a) the frequency region 3, and (b) the frequency region 6.

5. Experimental Result and Discussion

To experimentally examine the power flow of light into the crystal through the refraction at the surface,

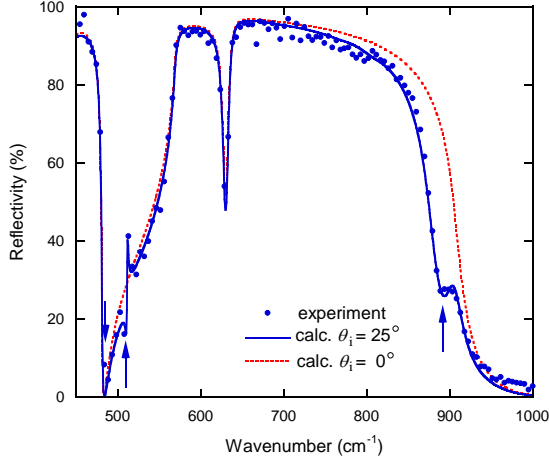


Fig. 14. (Color online) Experimental and calculated reflectivity spectrum in sapphire in the configuration *pac*. Arrows indicate positions of BNR expected when damping of phonons is negligibly small.

we measure the infrared reflection spectrum of sapphire in the configuration *pac* with θ_1 of $20^\circ \sim 40^\circ$. We employ an FTIR apparatus which is identical with that employed previously for the studies of small-angle oblique-incidence reflectometry^{17,18)} except that the beam-focusing equipment is replaced by the angle-variable one which is prepared for the present experiment. We also use one of the same synthetic crystals of sapphire from KYOCERA Corporation as those used in a previous study¹⁸⁾. The crystal is a plate with the *c*-face and a thickness of 0.33 mm.

Figure 14 shows the experimental result for $\theta_1 = 25^\circ$ in the configuration *pac* along with theoretical curves for $\theta_1 = 0^\circ$ and 25° . Half a reststrahlen band of the E_u^2 mode and the whole bands of the E_u^3 and E_u^4 modes are observed in the spectral range examined. The theoretical curves are calculated from eq. (21) with the phonon frequencies and damping energies listed in Table I. All the phonon frequencies and most of the damping energies are identical with those of ref. 18; only the damping energies of LO_{\parallel}^2 and LO_{\perp}^4 are adjusted by several wavenumbers. The experimental result is reproduced very well by the calculated curve. Compared with the theoretical curve for $\theta_1 = 0^\circ$, the spectrum for $\theta_1 = 25^\circ$ exhibits pronounced differences around 510 cm^{-1} and 900 cm^{-1} . A rapid drop of reflectivity to nearly null at 484.2 cm^{-1} and an asymmetric spike at 511.0 cm^{-1} arise from BNR and STR specific to the counterposition in the region 3, though the height of the spike is extremely suppressed by the damping of LO_{\parallel}^1 . On the other hand, the large

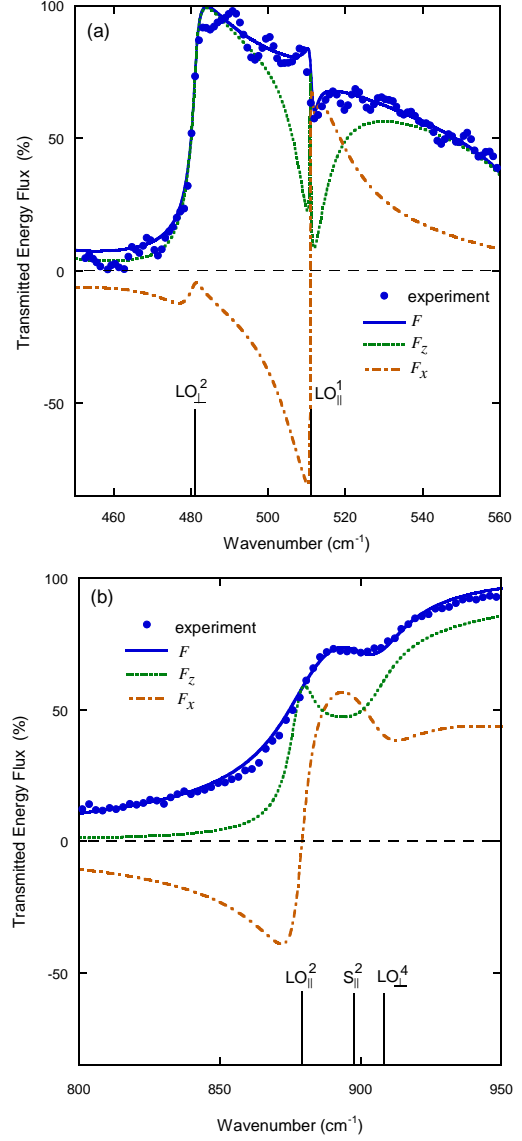


Fig. 15. (Color online) Experimental values of $1-R$ and theoretical curves of F , F_x , and F_z in sapphire for $\theta_1 = 25^\circ$ in the configuration *pac* around (a) the frequency region 3, and (b) the frequency region 6.

cut of the shoulder around 900 cm^{-1} shows the spectral transmission window which is produced by the negative refraction, and is promoted by BNR in the region 6. However, because of comparatively strong damping of LO_{\parallel}^2 and LO_{\perp}^4 , the observed transmittivity is insufficient in view of the calculated spectrum (see the spectrum for $\theta_1 = 20^\circ$ in Fig. 11). In the following, taking account of the damping of optical phonons, these observations are interpreted quantitatively in terms of the Poynting vector of the rays transmitted into the crystal.

Since the thickness, being 0.33 mm, of the crystal employed for the experiment is sufficiently large

compared with the reciprocal absorption coefficient, the measured quantity $1-R$ should be practically equal to the rate of the light flux transmitted into the crystal from the surface. The Poynting vector represents the energy flow per unit cross section per unit time, while in our experiment we measure the total energy flow per unit time of the incident and reflected light beams. Taking into account that the cross-sectional area of the light beam changes by a factor of $\cos\theta'_t/\cos\theta_i$ upon refraction, the power transmittance is given by

$$F = \frac{2c_0\varepsilon_0}{|H_{y0}^{(i)}|^2} \frac{\cos\theta'_t}{\cos\theta_i} |\bar{S}^{(t)}(0)|$$

$$= \frac{\cos\theta'_t}{\cos\theta_i} |\phi|^2 \left| \text{Re}\left[\frac{\sin\theta_i}{\varepsilon_z}\right] \mathbf{x} + \text{Re}\left[\frac{n_z^{(t)}}{\varepsilon_x}\right] \mathbf{z} \right|, \quad (30)$$

where $|\bar{S}^{(t)}(0)|$ is the absolute value of $\bar{S}^{(t)}$ at $z = 0$. The transmitted energy flux of light is composed of x and z components of

$$F_x = \frac{\cos\theta'_t}{\cos\theta_i} |\phi|^2 \text{Re}\left[\frac{\sin\theta_i}{\varepsilon_z}\right],$$

$$F_z = \frac{\cos\theta'_t}{\cos\theta_i} |\phi|^2 \text{Re}\left[\frac{n_z^{(t)}}{\varepsilon_x}\right]. \quad (31)$$

It is algebraically straightforward to prove $F = 1-R$. Figures 15(a) and 15(b) show the experimental values of $1-R$ around the regions 3 and 6, respectively, along with the curves of F , F_x , and F_z evaluated for $\theta_i = 25^\circ$ with $\varepsilon_x = \varepsilon_\perp$ and $\varepsilon_z = \varepsilon_\parallel$.

From experimental and calculated curves of F of Fig. 15(a), the spectral transmission window due to counterposition in the region 3 can be recognized to be present between LO_\perp^2 and LO_\parallel^1 . The ratio F_x/F_z indicates that $\theta'_t = -4.5^\circ$ at the frequency of LO_\perp^2 but the negative deflection of the energy flux is enhanced largely in the vicinity of LO_\parallel^1 to reach the largest negative deflection of $\theta'_t = -74^\circ$ at 510 cm^{-1} .

In the region 6, it is evident from Fig. 15(b) that negative refraction promotes the energy transmission of light into crystal. The hump around 890 cm^{-1} arises from BNR mentioned in §3, and the subsequent hollow around 900 cm^{-1} indicates the onset of STR which is expected to manifest itself between S_\parallel^2 and LO_\perp^4 when damping of phonons is small. If the damping is negligibly small, as mentioned in the argument on the criterion (b) in §2, the energy of the light beam continues to flow toward the positive

direction of x in the crystal, that is, the deflection of $\bar{S}^{(t)}$ is positive, even upon negative refraction of the waves. Interestingly, however, Fig. 15(b) shows that at frequencies below LO_\parallel^2 (879 cm^{-1}), being the lower boundary of the region 6, $\text{Re}[\varepsilon_\parallel]$ becomes negative, and thus F_x becomes negative. This fact means that the deflection of $\bar{S}^{(t)}$ becomes negative at frequencies below 879 cm^{-1} . We have already seen in Fig. 13(b) that a negative refraction of the real wave-normal vector is induced by damping additionally in a frequency region from 860 cm^{-1} up to 890 cm^{-1} . Consequently, $\bar{S}^{(t)}$ and the real wave-normal vector are simultaneously deflected and refracted negatively at frequencies between 860 cm^{-1} and 879 cm^{-1} . Hence, we may regard that a true negative refraction takes place there, although the penetration lengths of the plane waves and the rays are quite small because of a strong dissipation. As an example of this situation, Fig.16 illustrates the directions and penetration lengths of the wave and the ray at 875.0 cm^{-1} for $\theta_i = 25^\circ$.

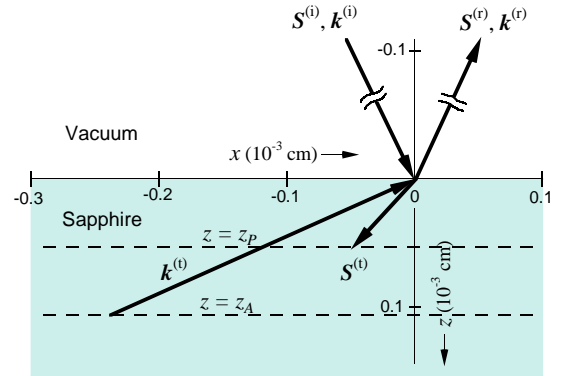


Fig. 16. (Color online) Wave vector \mathbf{k} and the Poynting vector \mathbf{S} of incident, reflected, and refracted infrared light with frequency 875.0 cm^{-1} in sapphire. The light is incident at $\theta_i = 25^\circ$ in the configuration *pac*. The head and the length of each arrow show the direction and the penetration length, respectively, of each vector. Dotted lines signified as $z = z_p$ and $z = z_A$ show the planes of penetration depths $1/\alpha$ and $2/\alpha$ of the Poynting vector and the wave vector, respectively.

6. Conclusions

Being prompted by the recent works on small-angle oblique-incidence reflectometry for ZnO and sapphire, we have studied the negative refraction phenomenon in natural crystals of uniaxial dielectric substances. The universal criteria characterizing the refraction behavior of light which is incident obliquely

to a nonabsorbing crystal are derived from Maxwell's equations. It is shown that the relative magnitudes and signs of the principal elements of the dielectric constant tensor are crucial for the refraction behavior of extraordinary rays. Applying the derived criteria to the infrared light dispersed by anisotropic multimode polar optical phonons in sapphire, it has been clarified how the negative refraction and counterposition arise as a function of the angle of incidence as well as the frequency of light. Anisotropic LO phonons are found to play major roles there through their contribution to the dielectric tensor.

The effect of damping of optical phonons on the refraction properties has been explored further to interpret the practical oblique-incidence reflection spectrum at the c -surface of a synthetic crystal of sapphire. The experimental spectrum demonstrates that spectral transmission windows are produced by counterposition and negative refraction in between evanescent regions. We have paid attention to the directions of the wave vector and the Poynting vector of the infrared light in the spectral range covering those transmission windows. The spectrum of the energy flux of light transmitted into the crystal, which is obtained by $1-R$ from the experimental reflection spectrum, is found to be explained successfully in terms of the frequency dependence of the direction of the Poynting vector. From this finding the waves and rays of infrared light turn out to be refracted and deflected simultaneously toward negative directions in a certain frequency range. This is the first experimental confirmation of a true negative refraction in a natural crystal.

The criteria obtained in the present study claim that the a -surface of sapphire exhibits different refraction behavior which is as rich in variety as the c -surface exhibits. Furthermore, any uniaxial dielectric substances other than sapphire will individually exhibit specific, unusual refractions.

Acknowledgements

The authors thank Dr. H. Tambo (AIST, Tsukuba) for his treatment of the surface of sapphire crystals used for the FTIR measurement. The present work was supported in part by a Grant-in-Aid for Scientific Research (No.17560024) from the Ministry of Education, Culture, Sports, Science and Technology of Japan.

-
- 1) V. G. Veselago: *Sov. Phys. Usp.* **10** (1968) 509.
 - 2) S. A. Ramakrishna: *Rep. Prog. Phys.* **68** (2005) 449.
 - 3) K. Cho: *Reconstruction of Macroscopic Maxwell Equations*, in *Springer Tracts in Modern Physics* (Springer-Verlag, Berlin Heidelberg, 2010) Vol. 237, Chap. 4.
 - 4) V. G. Veselago and E. E. Narimanov: *Nat. Mater.* **5** (2006) 759.
 - 5) V. M. Agranovich and Yu. N. Garstein: *Sov. Phys. Usp.* **49** (2006) 1029.
 - 6) I. V. Lindell, S. A. Tretyakov, K. I. Nikoskinen, and S. Ilvonen: *Microwave Opt. Technol. Lett.* **31** (2001) 129.
 - 7) P. A. Belov: *Microwave Opt. Technol. Lett.* **37** (2003) 259.
 - 8) D. R. Smith, W. J. Padilla, D. C. Vier, S. C. Nemat-Nasser, and S. Schultz: *Phys. Rev. Lett.* **84** (2000) 4184.
 - 9) J. B. Pendry: *Phys. Rev. Lett.* **85** (2000) 3966.
 - 10) R. A. Shelby, D. R. Smith, and S. Schultz: *Science* **292** (2001) 77.
 - 11) The progress in the optical study of metamaterials is reviewed in detail by V. M. Shalaev: *Nature Photonics* **1** (2007) 41.
 - 12) A. Lakhtakia and M. W. McCall: *Optik* **115** (2004) 28.
 - 13) V. A. Podolskiy and E. E. Narimanov: *Phys. Rev. B* **71** (2005) 201101.
 - 14) L. V. Alekseyev and E. Narimanov: *Opt. Express* **14** (2006) 11184.
 - 15) O. S. Eritsyan: *Crystallogr. Rep.* **50** (2005) 465.
 - 16) N. Kuroda and Y. Tabata: *J. Phys. Soc. Jpn.* **79** (2010) 024710.
 - 17) N. Kuroda, Y. Kumagai, T. Himoto, and H. Yokoi: *J. Phys. Soc. Jpn.* **79** (2010) 064712.
 - 18) Y. Kumagai, H. Yokoi, H. Tambo, Y. Tabata, and N. Kuroda: *J. Phys. Soc. Jpn.* **81** (2012) 024709.
 - 19) R. A. Depine, M. E. Inchaussandague, and A. Lakhtakia: *J. Opt. Soc. Am. A* **23** (2006) 949.
 - 20) M. Born and E. Wolf: *Principles of Optics* (Pergamon Press, New York, 1974) 5th ed., Chap. 14. This vector should be distinguished from the *ray-velocity* vector \mathbf{v} of which the direction is defined to be that of the Poynting vector, but the magnitude is defined by $\mathbf{n} \cdot \mathbf{v} = 1$.
 - 21) L. P. Mosteller, Jr. and F. Wooten: *J. Opt. Soc. Am.* **58** (1968) 511.
 - 22) D. R. Smith and D. Schurig: *Phys. Rev. Lett.* **90** (2003) 0774051.
 - 23) J. Lekner: *J. Opt. Soc. Am. A* **10** (1993) 2059.
 - 24) A. S. Barker, Jr.: *Phys. Rev.* **132** (1963) 1474.
 - 25) F. Gervais and B. Piriou: *J. Phys. C: Solid State Phys.* **7** (1974) 2374.
 - 26) A. K. Harman, S. Ninomiya, and S. Adachi: *J. Appl. Phys.* **76** (1994) 8032.
 - 27) M. Born and E. Wolf: *Principles of Optics* (Pergamon Press, New York, 1974) 5th ed., Chap. 1.
 - 28) M. C. Simon and K.V. Gottschalk: *Pure Appl. Opt.* **4** (1995) 27.
 - 29) K.V. Gottschalk and M. C. Simon: *J. Opt. Soc. Am. A* **18** (2001) 673.
 - 30) Y. J. Jen, A. Lakhtakia, C. W. Yu, and C. T. Lin: *Eur. J. Phys.* **30** (2009) 1381.
 - 31) V. A. Markel and J. C. Schotland: *J. Opt.* **12** (2010) 015104.

*Present address: Free Laboratory for Materials Technology,
Shimizunuma 2-10-18, Miyagino ward, Sendai 983-0845, Japan

‡Present address: Fujisawa Plant, Isuzu Motors Limited,
Fujisawa 252-0881, Japan

§E-mail address: kurodaflmt@ac.auone-net.jp